

## The effects of dilution and base plate strength on stress distributions in multi-pass welds deposited using low transformation-temperature filler alloys

T. I. Ramjaun<sup>a</sup>, H. J. Stone<sup>a</sup>, L. Karlsson<sup>b</sup>, J. Kelleher<sup>c</sup>, S. W. Ooi<sup>a</sup>, K. Dalaei<sup>d</sup>, J. Rebelo Kornmeier<sup>e</sup>, H. K. D. H. Bhadeshia<sup>a</sup>

<sup>a</sup>*Materials Science and Metallurgy, University of Cambridge, CB3 0FS, U.K.*

<sup>b</sup>*Engineering Science, University West, SE-461 86 Trollhättan, Sweden*

<sup>c</sup>*ISIS Facility, Rutherford Appleton Laboratory, Didcot, OX11 0QX, U.K.*

<sup>d</sup>*ESAB AB, Lindholmsallén 9, 40277, Gothenburg, Sweden*

<sup>e</sup>*Technische Universität München, Forschungsneutronenquelle Heinz Maier-Leibnitz (FRM II), 85747 Garching, Germany*

---

### Abstract

Transformation plasticity can be utilised to control residual stresses in steel welds. This requires special filler alloys that transform at a sufficiently low temperature to compensate for accumulated thermal contraction strains. However, the welding parameters needed to optimise the effect in multi-pass joints have yet to be established. This topic has been investigated by characterising the residual stress distribution in multi-pass welds fabricated with different welding alloys and base plates using neutron diffraction to assess the effects of dilution and base plate strength. Whilst the use of richly-alloyed weld metal does enhance fatigue performance in single-pass joints, the extent of stress relief that can be derived from transformation plasticity is reduced due to incomplete martensitic transformation when further layers are deposited. For all cases studied, compressive stresses were measured in the weld metal with balancing tensile stress in the heat-affected zone of the plate. The magnitude of the tension was observed to be a function of the strength of the base plate. Recommendations are also presented for the combination of welding and material parameters that lead to the optimum exploitation of transformation plasticity as a method for boosting the fatigue performance of multi-pass welded joints.

*Keywords:* transformation induced plasticity, martensitic weld metal, residual stress, welding, neutron diffraction

## 1. Introduction

Residual stresses that accumulate during the cooling of welded joints are an anathema in engineering design because they limit the loads that can be applied in service and often reduce fatigue performance. Post-weld treatments can be employed to counter these thermally induced stresses but an alternative method, proposed originally by Alberry and Jones [1], is to exploit the strains associated with solid-state phase transformation of the weld filler to cancel the thermal contraction [2–13]. This approach aims to improve the welding fabrication process through making expensive and labour intensive post-weld surface/heat treatments redundant.

As a weld cools, it contracts, producing harmful tensile residual stresses. However, the displacive nature of the austenite to martensite phase transformation ( $\gamma \rightarrow \alpha'$ ) is capable of negating these stresses and even producing compression in the weld metal. The details of this mechanism have been reviewed extensively elsewhere [14, 15] but an essential requirement of such weld filler alloys is that the transformation plasticity should not be exhausted until the weld cools to ambient temperature. This usually means that the weld metal should be designed to be martensitic with a low martensite-start temperature ( $M_S$ ). If transformation occurs at an elevated temperature, further thermal contraction will lead to a build up of tensile stress as the weld continues to cool, thus eliminating the initial stress relaxation benefits.

Naturally, other essential properties such as toughness and strength should not be compromised in the alloy design process [16, 17] and the carbon concentration must be low enough to avoid the embrittlement associated with hard martensite. With care, it is possible to reduce residual stresses in critical locations and enhance the fatigue strength of the joint [18–24]. Whilst much progress has been made in this field, open questions remain about the state of the joint when more than one layer of weld metal is deposited in order to fill the gap and the consequence of the multiple heat treatments experienced by underlying weld metal. The purpose of the work presented here is to elucidate these issues through characterisation of the residual stresses produced in multi-pass welds as a function of the transformation characteristics of the weld metal and the mechanical strength of the base plate.

## 2. Experimental Method

Six 3-pass welds were prepared from three different steel plates ('355'—a low strength structural steel, Weldox 700, Weldox 960) with three different welding consumables (LTT-1, LTT-2, Coreweld 89), as shown in Table 1. LTT-1 and LTT-2 are martensitic stainless steel filler alloys with a low  $M_S$ , whilst Coreweld 89 is a commercially available filler with a much higher  $M_S$ . Compositions of the plates and fillers are shown in Table 2. LTT-2 is highly alloyed and was designed to compensate for dilution, which inevitably occurs when the filler mixes with the base plate. The martensite-start temperature

of an undiluted sample of LTT-1 was measured using dilatometry and determined to be  $164 \pm 12^\circ\text{C}$ . This value is in agreement with the calculation by Steven & Haynes and the  $M_S$  of the undiluted alloys are also included in Table 2. The mechanical properties of the welding fillers and base plates are in Table 3, the LTT data are measured values.

Each of the welds was produced by mechanised gas-shielded metal arc welding (GMAW) on plates of dimensions  $500 \times 150 \times 15$  mm, machined with a  $60^\circ$  V-groove along the long direction and a root radius of 4 mm, Fig. 1. The plates were clamped to the bench prior to welding, which was performed horizontally in the down hand position with an initial pre-heat of  $50^\circ\text{C}$  and an inter-pass temperature of  $100\text{--}125^\circ\text{C}$ . All three welding alloys were deposited using metal-cored electrode wire with an Ar/CO<sub>2</sub> shielding gas. The heat input for the LTT and Coreweld 89 welding alloys was  $\sim 1.0$  and  $\sim 1.5$  kJ mm<sup>-1</sup> respectively.

It is the alloying additions that control the  $M_S$  of the filler so four plates were fabricated to understand the effects of weld metal dilution with the base plate. An additional two welds were prepared to determine the effects of base plate strength with respect to the filler.

### 2.1. Neutron Diffraction

The residual stresses in the welded plates were measured using neutron diffraction [25] on two strain scanning instruments: the STRESS-SPEC beamline [26] at the FRM II reactor (weld 4, 5, 6), and the ENGIN-X beamline [27] at the ISIS pulsed spallation neutron source (weld 1, 2, 3). For both experiments, strain scanning was performed across a plane perpendicular to the weld at the position along the sample shown in Fig. 2a. Measurements were made at 2.5, 5, 7.5, 10 and 12.5 mm below the top surface across both sides of the weld, heat-affected zone (HAZ) and base plate to identify any asymmetry in the stress field. It was assumed that the principal stresses are parallel to the plate edges.

The neutron diffraction techniques and subsequent stress analysis followed the same procedure as detailed elsewhere [28] but the key experimental parameters are shown in Table 4, where  $\lambda$  is the neutron wavelength,  $2\theta_M$  is the Bragg angle of the monochromator and  $V_V$  is the gauge volume for the appropriate measurement direction.

### 2.2. Stress Analysis

Strain-free reference specimens ('comb' samples) were used to account for the effect of compositional variation between the filler alloy and base plate for the measured lattice spacings. These were produced as 3 mm thick cross-sectional slices from the welded plate, Fig. 2a, and further slotted at 3 mm intervals along the transverse direction using wire electro-discharge machining (EDM), Fig. 2b. Due to the position of the EDM cuts, it was not possible to achieve perfect correspondence between the measurement positions in the welded plates and the combs. Therefore, a linear interpolation

was performed between the comb measurement positions at each depth to calculate the strain-free lattice spacings,  $d_{0,hkl}$ , for the relevant locations in the welded plates.

The elastic strain,  $\varepsilon_{hkl}$ , at each measurement location and direction was then found as follows:

$$\varepsilon_{hkl} = \frac{d_{hkl} - d_{0,hkl}}{d_{0,hkl}} \quad (1)$$

where  $d_{hkl}$ , is the interplanar spacing in the weld for a reflection ( $hkl$ ). Elastic strains were calculated from the ENGIN-X data in an analogous way using the lattice parameters.

The stress,  $\sigma_{ii}$ , in each of the three orthogonal directions was found from the strain measurements according to:

$$\sigma_{ii} = \frac{E}{(1 + \nu)} \left[ \varepsilon_{ii} + \frac{\nu}{(1 - 2\nu)} (\varepsilon_{11} + \varepsilon_{22} + \varepsilon_{33}) \right] \quad (2)$$

where  $E$  is the Young's modulus and  $\nu$  is Poisson's ratio.  $E = 220$  GPa and  $\nu = 0.28$  are the diffraction elastic constants for the  $\{211\}$  used to calculate the stress in welds 4, 5 and 6 [29].  $E = 212.7$  GPa and  $\nu = 0.30$  are the macroscopic bulk properties for a ferritic steel following the Kröner model and used to calculate the stress in welds 1, 2 and 3 [30].  $i = 1, 2, 3$  denotes the direction of the initial lattice parameter of lattice spacing measurement and hence, strain and stress direction with respect to the welded plate geometry.

### 3. Results and Discussion

#### 3.1. Residual Stress Measurements

Residual stresses were measured in the longitudinal, transverse and normal directions for each of the six welded plates, Fig. 3. The original measurement locations are indicated with crosses and the strains measured at these positions were used to map the stresses across the weld bead, HAZ and into the base plate at depths of 2.5–12.5 mm below the surface. Analogous to previous studies [6], the stress contours show symmetry across the centreline and follow the geometry of the weld.

Compressive stresses are evident in the weld material for all five specimens in the longitudinal direction that were welded with an LTT alloy. This is in contrast to weld 4 and confirms the shear and dilatational strains associated with the  $\gamma \rightarrow \alpha'$  transformation [6] at low temperature have compensated for the tensile thermal contraction strains, which would otherwise evolve. The stresses developed in the transverse and normal directions show evidence of compression in the LTT weld material but they are much lower in comparison. The longitudinally generated stresses are greatest because this is the direction of maximum thermal constraint during cooling. Weld 4 also appears to accumulate only minor compressive stresses in the weld bead

for the transverse and normal directions, although this is not necessarily an indication of low temperature transformation.

With respect to the longitudinal direction, the five LTT welds have a common stress distribution with compression in the weld metal nearer the surface and peak tensile stresses in the HAZ both below and either side of the weld. The tensile stresses are generated as a result of stress equilibration and the absence of low temperature  $\gamma \rightarrow \alpha'$  transformation in these locations. The re-austenitised regions in the base plate that surround the fusion boundary will transform to martensite at an elevated temperature, thus accumulating tensile residual stresses during the subsequent thermal contraction on cooling. Weld 4 shows a similar trend to the LTT welded plates but does not develop compressive stresses in the weld metal.

The stress contours are complemented by longitudinal-stress profiles, Fig. 4, which show the residual stresses at exact locations and are discussed in more detail in the sections that follow. The welds have been collated into two series, assessing the effects of dilution and base plate strength on residual stress with the view to improving fatigue performance. It is for this reason that particular attention is paid to the stresses nearest the specimen surface at the fusion boundary, where fatigue failure predominantly occurs. An additional figure is presented, Fig. 8, which investigates the issue of steep stress gradients across the fusion boundary/HAZ and the number of measurement positions necessary to adequately describe the stress change.

### *3.2. The Effects of Dilution*

Welds 4, 1 and 2 were welded with increasingly-alloyed filler metals and hence, decreasing  $M_S$ . Weld 3 comprised of three layers with only the final, capping pass being an LTT alloy, to ascertain the possibility of influencing the surface residual stresses whilst minimising the use of these relatively expensive materials. Although the stress state is evaluated throughout the entire weld in three orthogonal directions, emphasis is placed on the longitudinal stresses nearest the top surface due to these stresses being the greatest in magnitude and the surface region being the predominant initiation site for fatigue failure.

Weld 4 was fabricated with a conventional high  $M_S$  filler alloy and shows the expected tensile stresses in the fusion zone that are generated because the  $\gamma \rightarrow \alpha'$  transformation occurs at a relatively high temperature, thus allowing further thermal contraction strains to develop after the transformation is exhausted. A large region of high tensile stress (+600 MPa) envelops the majority of the HAZ, extending to the measurement position nearest the top surface. This is in contrast to welds 1 and 2, which generate compression in the weld metal and have much smaller regions of tensile stress above 600 MPa that are situated further from the top surface. Weld 3 also develops compressive stress in the final LTT alloy capping pass.

Due to the tensile stresses developed in the weld metal for weld 4 and the compression (-200 MPa) in the same region for weld 1 (low  $M_S$  filler), it

might be expected that weld 2, which has an even lower  $M_S$ , exhibit greater compressive stresses. The data for welds 4, 1 and 2 (Fig. 7) are inconsistent with this hypothesis because the magnitude of compressive residual stress in weld 1 is greater than weld 2. This is caused by untransformed austenite in weld 2 resulting from the heavily alloyed LTT-2 filler with a suppressed  $M_S$  [31]. The full extent of transformation plasticity clearly cannot be achieved with the partial transformation of austenite so only minor compressive stresses are produced in weld 2.

In order to illustrate this point, Fig. 5 provides a schematic diagram of the effect of  $M_S$  on the residual stresses produced in three different welding alloys during a constrained cooling situation. A bar of each alloy is cooled from a stress-free state at high temperature with the ends of the bar fixed, preventing any thermal shrinkage. This is an idealised model of the constrained cooling that occurs in the weld and HAZ during welding [32]. The welding filler with a high  $M_S$  transforms prematurely, which leads to tensile residual stress in the weld metal as it continues to thermally contract until it reaches ambient temperature. The filler with an overly suppressed  $M_S$ , such that the  $\gamma \rightarrow \alpha'$  transformation is largely incomplete at ambient temperature, achieves only partial stress relaxation. Although, this is preferable to tensile residual stress. The 'ideal' filler transforms at the optimum temperature to allow complete transformation, which results in maximum stress alleviation to the extent of inducing large compressive stress in the weld metal.

The macrograph in Fig. 6 shows evidence of continuous columnar grains growing across the fusion boundary between welding passes 2–3, which would indicate that the  $M_S$  of the weld bead in this region is similar to the inter-pass temperature [28]. The welding alloy developed by Karlsson *et al.* [21] to compensate for dilution with the base plate displays greater fatigue performance than the standard LTT alloy. Importantly, this is for single-pass welds where the extent of dilution is typically 30% and elevates the  $M_S$ . However, LTT-2 may be not suitable as the sole filler for multi-pass welds since its undiluted  $M_S$  is too low for complete transformation.

Weld 3, which incorporated a single capping pass of LTT-2, shows the desired accumulation of compressive stresses in the LTT weld metal but the remainder of the stress distribution is synonymous with weld 4. Tensile stresses are evident around the HAZ at the measurement positions nearest the surface and Fig. 7 suggests that the maximum tensile stress for weld 3 is the same as that for weld 4. Although the final LTT-2 capping pass is unable to reverse the effects of accumulated tensile stress in the initially deposited layers of the high  $M_S$  filler and surrounding HAZ, compressive stresses were developed in the LTT weld metal. Similarities between the maximum tensile stress and distributions of weld 3 and 4 are evident for this work, however, the residual stress states at the actual surface could deviate.

Weld 1 and 2 appear to have the most favourable stress distributions (compared with weld 4 and 3) based on smaller regions of high tensile stress further below the top surface. Despite the benefits to fatigue performance

with a single-pass, multi-pass welds produced with the highly alloyed LTT-2 may not be appropriate because of the mechanical properties associated with high levels of retained austenite. In addition, results from an investigation into the effects of inter-pass temperature ( $T_1$ ) [28] for the filler LTT-1 show a further improvement of stress distribution when the  $T_1 > M_S$ . Depending on the welding speed and number/geometry of passes, it is possible that the entire weld will subsequently transform simultaneously on cooling, thus realising the full benefits of transformation plasticity across the entire weld.

### *3.3. Effects of Base Plate Strength*

In order to determine the versatility of the LTT alloys with regards to welding steel plates of varying strength, two base materials were selected that had yield strengths above (weld 5) and below (weld 6) that of the filler alloy. For weld 1, the yield strength of the filler was comparable to the base plate and the mechanical properties are listed in Table 3. All of the welds show compression in the weld metal and maximum tensile stresses in the vicinity of the HAZ that correlate with the yield strength of the associated base plate. This would suggest that the thermal stresses generated in the constrained weld metal and surrounding base plate approach or exceed the yield strengths of the respective materials, although there is likely to be some difference in microstructure/properties between the HAZ and unaffected base plate. Remarkably, the phase transformation in the LTT weld metal is sufficient to negate the tensile stresses that develop in the fusion zone. However, the accumulated tensile stresses in the base plate remain, although expansion of the weld metal will inevitably lead to some alleviation and re-distribution.

Comparing the stress distribution in the HAZ for welds 1 and 4, both deposited on Weldox 700, there is a significant reduction in the magnitude of tensile stress when the LTT welding alloy is used. Applying this principle to weld 5, which has a small region of tensile stress in excess of 800 MPa, it is possible that the entire HAZ will be above this value when welding with a conventional filler.

### *3.4. Strain Measurement Positions*

As a result of the time limitations associated with strain scanning using neutron diffraction, a compromise usually exists between the number of measurement positions and the number of specimens that can be analysed. Additional strain measurements were taken for weld 5, Fig. 8, to ensure that the initial concentration of points was sufficient to adequately capture the stress profiles across regions of abrupt change, such as the fusion boundary and HAZ. For the collection of welds in this work, readings were taken every 3 mm, signified by the solid markers. Additional points have been included (open markers) to show the change in profile for measurement positions every 1 mm. The initial concentration of points provides a satisfactory representation of the stress changes that occur for the scope of this work, but they do not capture the exact locations of the inflections and

the maximum/minimum values, which can deviate over 100 MPa from those originally measured.

#### 4. Conclusions

A study of the residual stresses produced following the welding of a series of ferritic steel plates with low transformation-temperature filler alloys has been performed using neutron diffraction. From this study the following conclusions and recommendations have been drawn:

- There appears to be no additional benefit to stress relief by using a highly enriched welding filler (LTT-2) to compensate for compositional dilution with the base plate for multi-pass welds. This is due to an overly suppressed  $M_S$  such that the  $\gamma \rightarrow \alpha'$  transformation cannot be fully exploited at ambient temperatures in the final passes.
- The use of a highly enriched welding filler (LTT-2) as a final capping pass successfully imparts minor compression into the surface regions of the deposited weld metal, however, large regions of high tensile stresses remain in the surrounding HAZ.
- Compressive stresses were generated in the weld metal for a series of base plates that have differing yield strengths, above and below that of the LTT filler. However, residual stresses approximately equal to the yield strength of the base plate remained in the regions surrounding the HAZ. The re-austenised base plate material surrounding the fusion boundary will inevitably transform to martensite at an elevated temperature, which will lead to the accumulation of tensile stresses due to the high  $M_S$  of the plate.
- The present work indicates that higher spatial-resolution ( $\approx 1$  mm) measurements of the stresses are necessary in order to adequately capture the positions of inflection and the maximum/minimum stresses across the fusion boundary and HAZ.
- It is believed that weld 1 provides the optimum stress distribution based on the maximum tensile stresses generated with respect to the yield strength of the base plate and the relative sizes and positions of these high tensile regions. Although weld 2 produces a comparable stress distribution, the retained austenite in the final passes will reduce the strength of the weld metal in this region. However, this may be beneficial if a particularly tough and ductile weld is preferred.

#### Acknowledgments

We are grateful to ESAB AB for sponsoring this research. This work is based upon experiments performed on the ENGIN-X instrument at ISIS, Rutherford Appleton Laboratory, Didcot, U.K. (RB 1220125) and the STRESS-SPEC instrument operated by FRM II at the Heinz Maier-Leibnitz Zentrum (MLZ), Garching, Germany.



## References

1. W. K. C. Jones, and P. J. Alberry: 'A model for stress accumulation in steels during welding', *Metals Technology*, 1977, **11**, 557–566.
2. A. Ohta, N. Suzuki, Y. Maeda, K. Hiraoka, and T. Nakamura: 'Superior fatigue crack growth properties in newly developed weld metal', *International Journal of Fatigue*, 1999, **21**, S113–S118.
3. J. Eckerlid, T. Nilsson, and L. Karlsson: 'Fatigue properties of longitudinal attachments welded using low transformation temperature filler', *Science and Technology of Welding and Joining*, 2003, **8**, 353–359.
4. H. Lixing, W. Dongpo, W. Wenxian, and Y. Tainjin: 'Ultrasonic peening and low transformation temperature electrodes used for improving the fatigue strength of welded joints', *Welding in the World*, 2004, **48**, 34–39.
5. S. Zenitani, N. Hayakawa, J. Yamamoto, K. Hiraoka, Y. Morikage, T. Yauda, and K. Amano: 'Development of new low transformation temperature welding consumable to prevent cold cracking in high strength steel welds', *Science and Technology of Welding and Joining*, 2007, **12**, 516–522.
6. J. A. Francis, H. J. Stone, S. Kundu, R. B. Rogge, H. K. D. H. Bhadeshia, P. J. Withers, and L. Karlsson: 'Transformation temperatures and welding residual stresses in ferritic steels', In: *Proceedings of PVP2007, ASME Pressure Vessels and Piping Division Conference*. American Society of Mechanical Engineers, San Antonio, Texas: ASME, 2007:1–8.
7. P. P. Darcis, H. Katsumoto, M. C. Payares-Asprino, S. Liu, and T. A. Siewert: 'Cruciform fillet welded joint fatigue strength improvements by weld metal phase transformations', *Fatigue and Fracture of Engineering Materials and Structures*, 2008, **31**, 125–136.
8. M. C. Payares-Asprino, H. Katsumoto, and S. Liu: 'Effect of martensite start and finish temperature on residual stress development in structural steel welds', *Welding Journal, Research Supplement*, 2008, **87**, 279s–289s.
9. H. Dai, J. A. Francis, H. J. Stone, H. K. D. H. Bhadeshia, and P. J. Withers: 'Characterising phase transformations and their effects on ferritic weld residual stresses with X-rays and neutrons', *Metallurgical & Materials Transactions A*, 2008, **39**, 3070–3078.
10. Y. Mikami, Y. Morikage, M. Mochizuki, and M. Toyoda: 'Angular distortion of fillet welded T joint using low transformation temperature welding wire', *Science and Technology of Welding and Joining*, 2009, **14**, 97–105.

11. A. Kromm, and T. Kannengiesser: ‘Characterising phase transformations of different LTT alloys and their effect on residual stresses and cold cracking’, *Welding in the World*, 2011, **55**, 48–56.
12. J. Altenkirch, J. Gibmeler, A. Kromm, T. Kannengiesser, T. Nitschke-Pagel, and M. Hofmann: ‘In situ study of structural integrity of low transformation temperature (LTT)-welds’, *Materials Science & Engineering A*, 2011, **528**, 5566–5575.
13. T. Kasuya, Y. Hashiba, H. Inoue, T. Nose, K. Ito, and M. Enoki: ‘Cold cracking susceptibility of austenitic and martensitic weld metals’, *Welding in the World*, 2012, **56**, 76–84.
14. J. A. Francis, H. K. D. H. Bhadeshia, and P. J. Withers: ‘Welding residual stresses in ferritic power plant steels’, *Materials Science and Technology*, 2007, **23**(9), 1009–1020.
15. S. W. Ooi, J. E. Garnham, and T. I. Ramjaun: ‘Low transformation temperature weld filler for tensile residual stress reduction’, *Materials and Design*, 2014, **56**, 773–781.
16. A. A. Shirzadi, H. K. D. H. Bhadeshia, L. Karlsson, and P. J. Withers: ‘Stainless steel weld metal designed to mitigate residual stresses’, *Science and Technology of Welding and Joining*, 2009, **14**, 559–565.
17. R. J. Moat, H. J. Stone, A. A. Shirzadi, J. A. Francis, S. Kundu, A. F. Mark, H. K. D. H. Bhadeshia, L. Karlsson, and P. J. Withers: ‘Design of weld fillers for mitigation of residual stresses in ferritic and austenitic steel welds’, *Science and Technology of Welding and Joining*, 2011, **16**, 279–284.
18. J. A. Francis, M. Turski, and P. J. Withers: ‘Measured residual stress distributions for low and high heat input single weld beads deposited on to SA508 steel’, *Materials Science and Technology*, 2009, **25**, 325–334.
19. J. A. Francis, H. J. Stone, S. Kundu, H. K. D. H. Bhadeshia, R. B. Rogge, P. J. Withers, and L. Karlsson: ‘Effects of filler metal transformation temperature on residual stresses in a high strength steel weld’, *Journal of Pressure Vessel Technology*, 2009, **131**, 0414011–0414018.
20. L. Karlsson, L. Mráz, H. K. D. H. Bhadeshia, and A. Shirzadi: ‘Alloying concepts for low transformation temperature welding consumables’, *Biuletyn Instytutu Spawalnictwa*, 2010, **5**, 33–39.
21. L. Karlsson, and L. Mráz: ‘Increasing fatigue life with low transformation temperature (LTT) welding consumables’, *Zváranie svarováni*, 2011, **1–2**, 8–15.
22. C. Miki, T. Hanji, and K. Tokunaga: ‘Weld repair for fatigue-cracked joints in steel bridges by applying low temperature transformation welding wire’, *Welding in the World*, 2012, **56**, 40–50.

23. M. Takahashi, and H. Y. Yasuda: ‘Variant selection of martensites in steel welded joints with low transformation temperature weld metals’, *Journal of Alloys and Compounds*, 2013, **577**, S601–S604.
24. C. Miki, and T. Masayuki: ‘Fatigue strength improvement of out-of-plane welded joints of steel girder under variable amplitude loading’, *Welding in the World*, 2013, **57**, 823–840.
25. M. E. Fitzpatrick, and A. Lodini, eds.: Analysis of residual stress by diffraction, using neutron and synchrotron radiation: Florida, USA: CRC Press LLC, 2003.
26. M. Hofmann, R. Schneider, G. A. Seidl, J. Rebelo-Kronmeier, R. Wimporoy, U. Grabe, and H. G. Brokmeier: ‘The new materials science diffractometer STRESS-SPEC at FRM-II’, *Materials Science Forum*, 2006, **524–525**, 211–216.
27. J. R. Santisteban, M. R. Daymond, J. A. James, and L. Edwards: ‘ENGIN-X: a third-generation neutron strain scanner’, *Journal of Applied Crystallography*, 2006, **39**, 812–825.
28. T. I. Ramjaun, H. J. Stone, L. Karlsson, J. Kelleher, R. J. Moat, J. R. Kornmeier, K. Dalaei, and H. K. D. H. Bhadeshia: ‘Effect of inter-pass temperature on residual stresses in multi-pass welds produced using a low transformation temperature filler alloy’, *Science and Technology of Welding and Joining*, 2014, **19**, 44–51.
29. B. Eigenmann, and E. Macherauch: ‘Röntgenographische untersuchung von spannungszuständen in werkstoffen. teil iii. fortsetzung von matwiss. und werkstofftechn’, *Materialwissenschaft und Werkstofftechnik*, 1996, **27**, 426–437.
30. M. T. Hutchings, P. J. Withers, T. M. Holden, and T. Lorentzen: Introduction to the characterization of residual stress by neutron diffraction: Florida, USA: CRC Press, 2005.
31. W. Wang, L. Huo, Y. Zhang, D. Wang, and H. Jiang: ‘New developed welding electrode for improving the fatigue strength of welded joints’, *Journal of Materials Science and Technology*, 2002, **18**, 527–531.
32. K. Satoh: ‘Transient thermal stresses of weld heat-affected zone by both-ends-fixed bar analogy’, *Kovove Materialy*, 1970, **8**, 569–587.

Table 1: Combinations of welding consumables and base plates.

Weld	Base Plate	Pass 1	Pass 2	Pass 3
1	Weldox 700	LTT-1	LTT-1	LTT-1
2	Weldox 700	LTT-2	LTT-2	LTT-2
3	Weldox 700	Coreweld 89	Coreweld 89	LTT-2
4	Weldox 700	Coreweld 89	Coreweld 89	Coreweld 89
5	Weldox 960	LTT-1	LTT-1	LTT-1
6	355	LTT-1	LTT-1	LTT-1

Table 2: Compositions (wt %) and  $M_S$  of the undiluted welding alloys and base plates. The LTT  $M_S$  were calculated based on a measured composition.

Material	C	Si	Mn	Cr	Ni	Mo	Calculated $M_S$ (°C)
LTT-1	0.01-0.03	0.6-0.8	1.2-1.7	12.5-13.0	5.5-6.5	<0.1	169
LTT-2	<0.02	<1	<2	15-18	6-8	<0.1	87
Coreweld 89	0.12	0.65	1.50	0.70	2.80	0.85	372
Weldox 700	0.15	0.29	0.98	0.25	0.043	0.15	447
Weldox 960	0.17	0.22	1.24	0.2	0.052	0.65	420
355	0.16	0.26	0.95	0.012	0.017	<0.01	451

Table 3: Mechanical properties of the undiluted welding alloys and base plates.

Material	0.2% stress (MPa)	Tensile strength (MPa)	Elongation (%)	Impact energy (at -20°C)
LTT-1	627	1111	14.0	45
LTT-2	316	845	31.8	88
Coreweld 89	>900	> 900	19.0	>90
Weldox 700	>700	780-930	14.0	>27
Weldox 960	>960	980-1150	12.0	>27
355	>355	470-630	22.0	>27

Table 4: Experimental parameters for stress measurements by neutron diffraction.

Parameter	ENGIN-X	STRESS-SPEC
$\lambda$	Time-of-flight	$\sim 1.69 \text{ \AA}$
Diffraction peak	Multiple	{211}
$2\theta_M$	$76-104^\circ$	$77.3^\circ$
Longitudinal $V_v$	$3 \times 3 \times 3 \text{ mm}^3$	$2 \times 2 \times 2 \text{ mm}^3$
Transverse $V_v$	$3 \times 15 \times 3 \text{ mm}^3$	$2 \times 20 \times 2 \text{ mm}^3$
Normal $V_v$	$3 \times 15 \times 3 \text{ mm}^3$	$2 \times 20 \times 2 \text{ mm}^3$

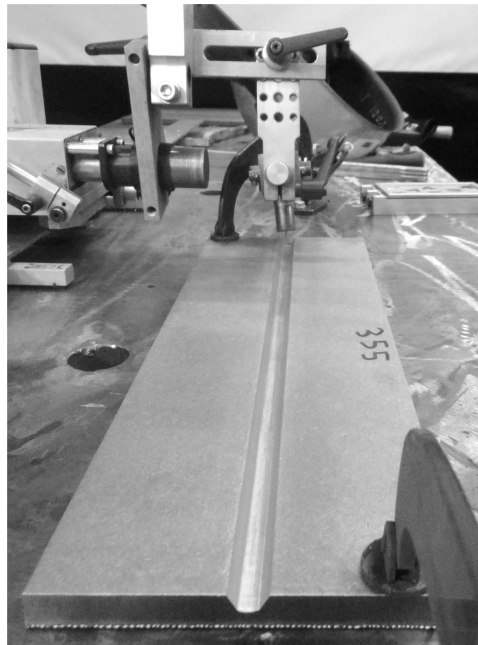


Figure 1: Machined plate set-up for welding.

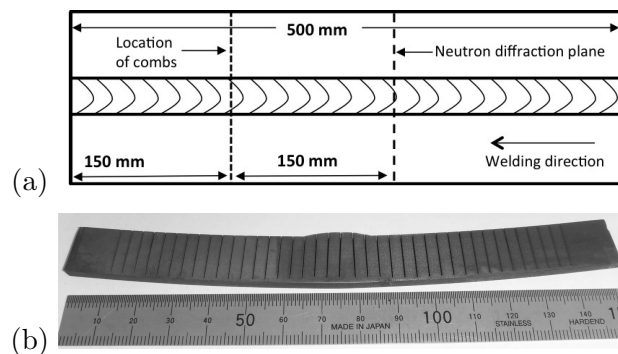


Figure 2: (a) Plan view of a welded plate showing the locations of the residual strain measurements and reference strain-free specimens. (b) Sectioned specimen used to determine the strain-free lattice parameter [28].

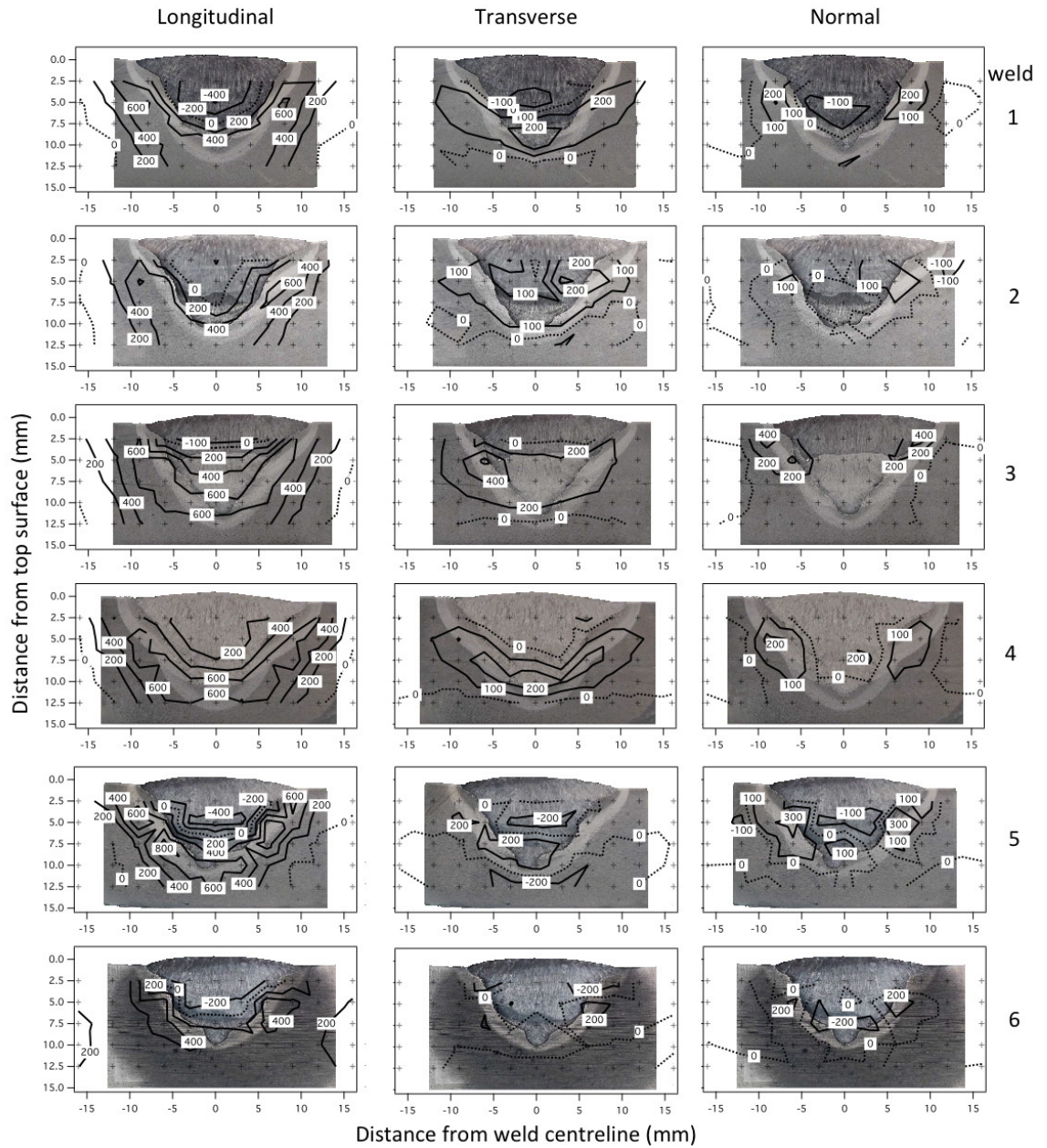


Figure 3: Residual stress contours, in MPa, for the six different welds.

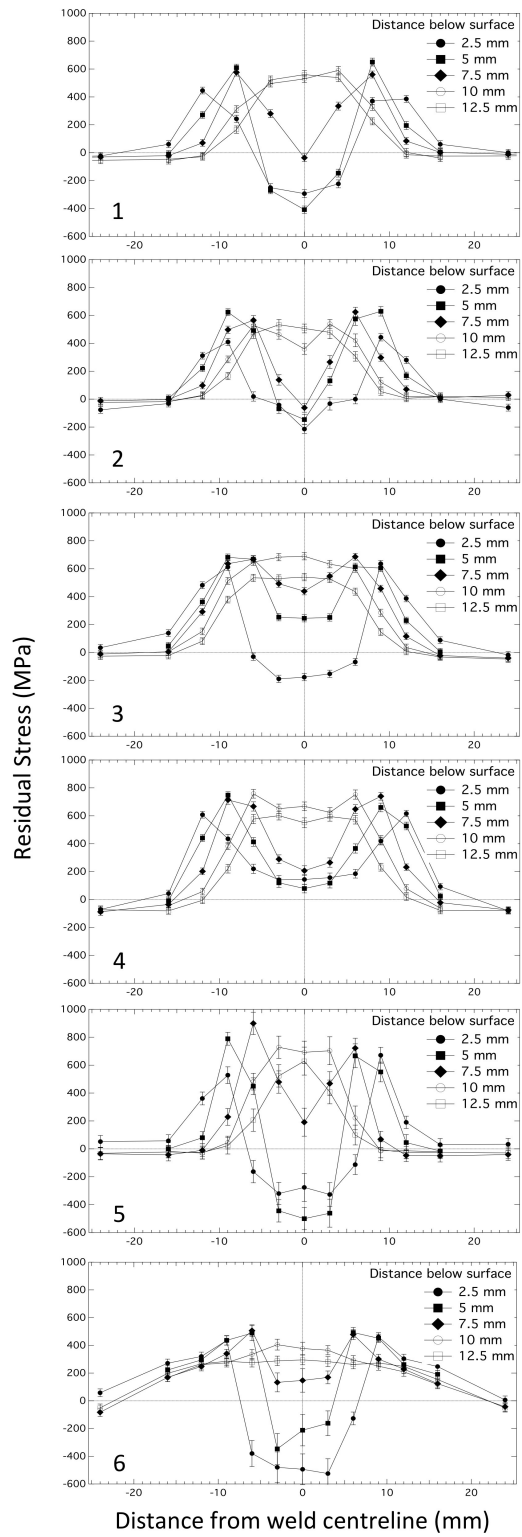


Figure 4: Longitudinal residual stress profiles as a function of distance from the weld centreline.

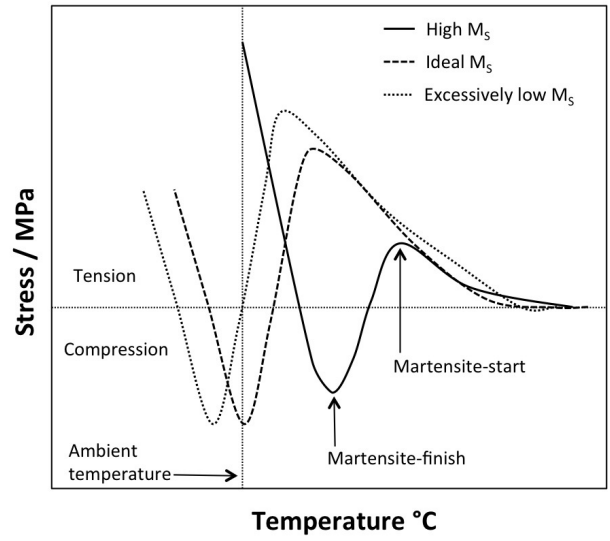


Figure 5: Schematic illustration of the residual stresses for three welding alloys with differing  $M_S$ , highlighting the effect of an overly suppressed  $M_S$ .

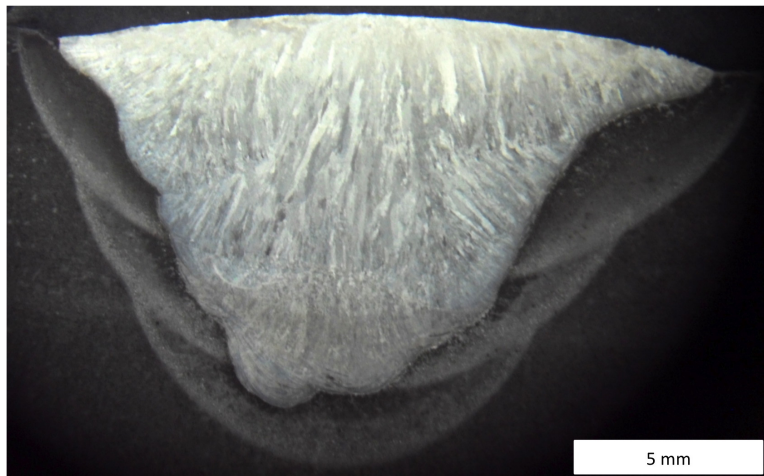


Figure 6: Macrostructure of weld 2 revealed using ferric chloride.



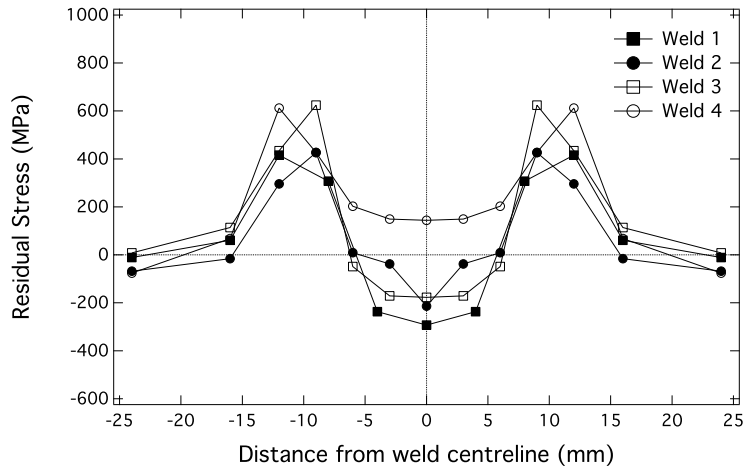


Figure 7: Welds 1, 2, 3, 4: Averaged longitudinal residual stress profiles at 2.5 mm below the top surface as a function of distance from the weld centreline.

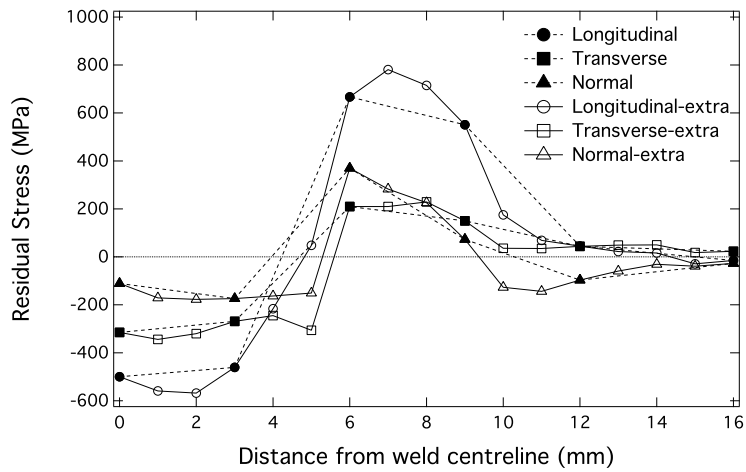


Figure 8: Weld 5: Longitudinal, transverse and normal residual stress profiles as a function of distance from the weld centreline highlighting the change in profile with additional strain measurement positions at 5 mm below the surface.